AIP Advances

Structural, electronic, magnetic, and optical investigations of sodium chalcogenides: First-principles calculations

Cite as: AIP Advances **13**, 015110 (2023); https://doi.org/10.1063/5.0129392
Submitted: 04 October 2022 • Accepted: 19 December 2022 • Published Online: 06 January 2023

Raed T. Jaradat, Mohammed S. Abu-Jafar, Mahmoud Farout, et al.

Structural, electronic, magnetic, and optical investigations of sodium chalcogenides: First-principles calculations

Cite as: AIP Advances 13, 015110 (2023); doi: 10.1063/5.0129392
Submitted: 4 October 2022 • Accepted: 19 December 2022 •
Published Online: 6 January 2023

Raed T. Jaradat,[1,2,a)] Mohammed S. Abu-Jafar,[1,a)] Mahmoud Farout,[1] Said M. Azar,[3] Rabah Khenata,[4] and Ahmad A. Mousa[5,6]

AFFILIATIONS

[1] Physics Department, An-Najah National University, Nablus, Palestine
[2] Palestinian Ministry of Education and Higher Education, Ramallah, Palestine
[3] Department of Physics, Faculty of Science, Zarqa University, 13132 Zarqa, Jordan
[4] Laboratoire de Physique Quantique et de Modélisation Mathématique de la Matière (LPQ3M), Université de Mascara, Mascara 29000, Algeria
[5] Middle East University, Amman 11831, Jordan
[6] Applied Science Research Center, Applied Science Private University, Amman, Jordan

[a)] **Authors to whom correspondence should be addressed:** raieddd@hotmail.com and mabujafar@najah.edu

ABSTRACT

The electronic, magnetic, and optical properties of NaS and NaSe compounds have been studied by using first-principles calculations based on density-functional theory and full-potential linearized augmented plane-wave method. The Perdew–Burke–Ernzerhof generalized gradient approximation (PBE-GGA) and modified Becke–Johnson (mBJ-GGA) have been used to deal with the exchange-correlation potential. The PBE-GGA and mBJ-GGA electronic calculation of the spin-up configuration shows an insulating behavior, while the spin-down shows a metallic behavior. In addition, both PBE-GGA and mBJ-GGA agree that the total magnetic moment per unit cell for these compounds is 1 μB. From optical calculations, we see that $\varepsilon_1(0)$ value in the spin-up channel is positive, which shows an insulating character, while it has a large negative value for the spin-down configuration, which shows a metallic character. The NaS and NaSe refractive index $n(\omega)$ indicates a metallic demeanor as the real and imaginary parts of the dielectric constant.

I. INTRODUCTION

Half-metallic ferromagnetic (HMF) compounds or alloys, where one spin band direction shows a semiconducting or insulating behavior with a gap at the Fermi level F_E, while the other spin band direction shows a metallic behavior, have attracted increasing interest. In high performance spintronic devices, the HMF compounds are seen as a key ingredient since they may show full spin polarization with only one electronic spin direction at the F_E.[1,2] These HMF compounds are expected to be suitable for room temperature spintronic applications. The rapid growth of research on HMF compounds has found that they are suitable for spintronic devices.[3] HMF compounds have been theoretically and experimentally studied for a wide range of compounds and alloys, such as Heusler alloys, perovskite manganite, and zincblende transition-metal.

The first prediction of HMF of the half-Heusler alloy NiMnSb was studied in 1983 by de Groot *et al.*[4] Since then, different types of HMF compounds or alloys have been predicted. Ishida *et al.*[5] predicted the HMF behavior for CoVSb alloy, while Weht and Pickett[6] predicted the HMF behavior for Mn_2VAl alloy. Furthermore, HMF compounds were predicted in some magnetic oxides such as Fe_3O_4[7] and CrO_2.[8] Diluted magnetic semiconductor alloys such as $Ga_xMn_{1-x}N$[9] and $Zn_xCo_{1-x}O$[10] show HMF behavior. Some

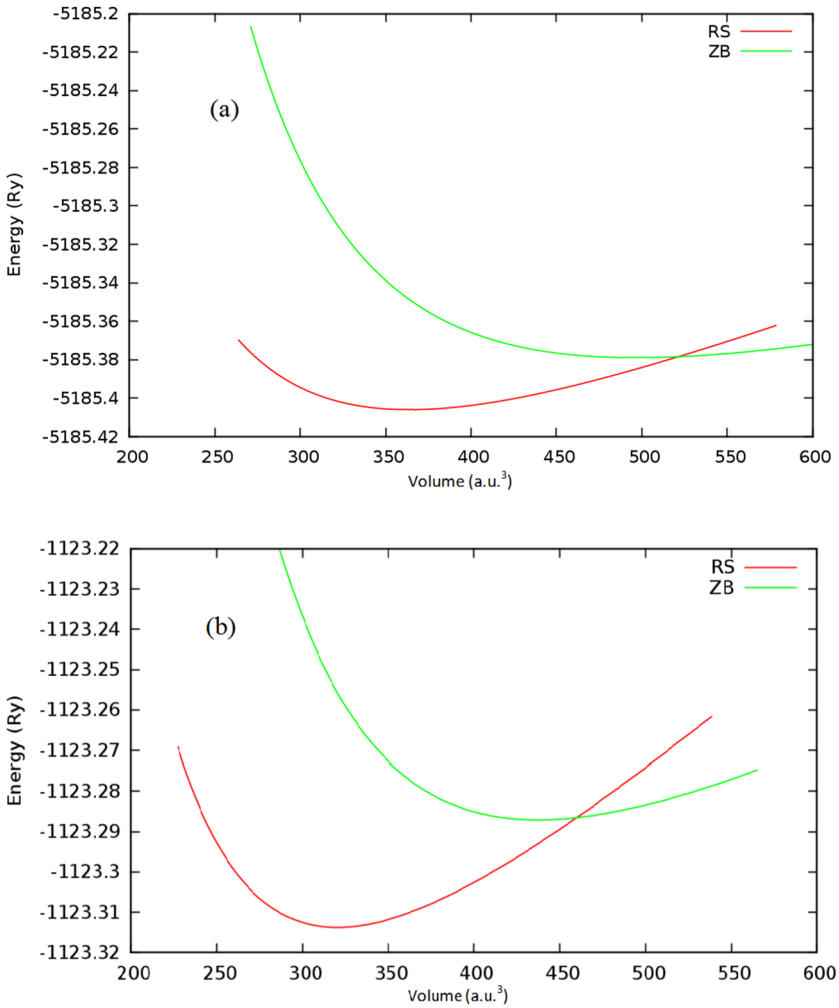

FIG. 1. Calculated total energy per unit cell vs cell volume for (a) NaSe and (b) NaS compounds.

zincblende (ZB) transition-metals such as CrTe[11] and CrSe[12] show HMF behavior.

Dahliah *et al.*[13] calculated the total energy and the mechanical elastic properties for PtC and showed that the PtC compound crystallizes in the ZB structure at ambient conditions. Recently, Abu-Jafar *et al.*[14] predicted that the ScS and ScSe compounds have a metallic behavior in all studied phases. Furthermore, they found that the NiAs phase is the ground state of ScSe, while the rock

TABLE I. Structural parameters of NaS and NaSe compounds along with other theoretical results.

		ZB structure		RS structure	
Compound	Structural parameters	Present work	Other theoretical work	Present work	Other theoretical work
NaS	a_0 (Å)	6.3763	6.39[a], 6.38[b]	5.748	5.76[a], 5.75[b]
	B_0 (GPa)	15.48	16[a], 15[b]	24.56	24[a], 24[b]
	B'_0	4.78	4.49[a], 3.36[b]	4.56	3.77[a], 4.45[b]
NaSe	a_0 (Å)	6.653	6.67[a], 6.65[b]	5.997	6.0[a], 6.0[b]
	B_0 (GPa)	13.4	14.0[a], 13.0[b]	21.39	20[a], 21[b]
	B'_0	4.69	4.52[a], 3.48[b]	4.228	4.5[a], 3.79[b]

[a]Reference 17.
[b]Reference 19.

salt (RS) phase is the ground state of ScS. Han *et al.*[15] studied the magnetic and electronic properties of alkali (K, Na, and Li) doped AlN. They found that the spin polarized state is more favorable than the non-spin polarized state: the spin polarized state has lower energy. Few studies have been performed to determine the structural and electronic properties of sodium based chalcogenides NaM (M = S, Se, and Te).[16,17] Gao *et al.*[16] used full-potential linearized augmented plane-wave (FP-LAPW) method within generalized gradient approximation (GGA) to calculate the structural, electronic, and magnetic properties of XS (X = K, Li, and Na) in ZB and RS structures. They concluded that the RS structure of NaS and KS is HMF. Ahmadian[17] carried out the FP-LAPW approach within spin polarized density functional theory to compute the electronic and magnetic properties of NaX compounds (X = O, S, Se, Te, and Po) in RS, ZB, and NiAs structures. The NaX compounds (X = S, Se, and Te) in the ZB and RS structures were found to be HMF. Moradi *et al.*[18] used the pseudopotential self-consistent method based on density functional theory (DFT) to investigate the magnetic properties of MS (M = Na, K, and Li) compounds in the wurtzite (WZ) structure. They found that LiS, NaS, and KS compounds are HMF and maintain their half-metallic behavior under pressure to a certain amount. Sadouki *et al.*[19] used FP-LAPW to investigate the structural, electronic, and magnetic properties of NaS, NaSe, and NaTe compounds. These compounds in ZB and WZ structures show a half-metallic behavior, and their magnetic moment was calculated to be 1 μB per unit cell.

In this study, we investigated the structural, electrical, magnetic, and optical characteristics of NaX (X = S and Se) compounds in the ZB and RS crystalline structures. In addition, the induced transition pressure effect is studied.

The exchange-correlation potential for the electronic and optical properties was calculated by using PBE-GGA and mBJ-GGA approaches. To the best of our knowledge, there are no experimental work and previous theoretical investigations for the induced transition pressure and optical properties of the alkali-metal chalcogenides, NaS and NaSe compounds, reported in the literature. Moreover, the electronic and magnetic properties are not experimentally available in the literature for alkali-metal chalcogenides (NaS and NaSe compounds). This paper can be considered as a prediction study, and we expect that our study will motivate some other optical works on these compounds.

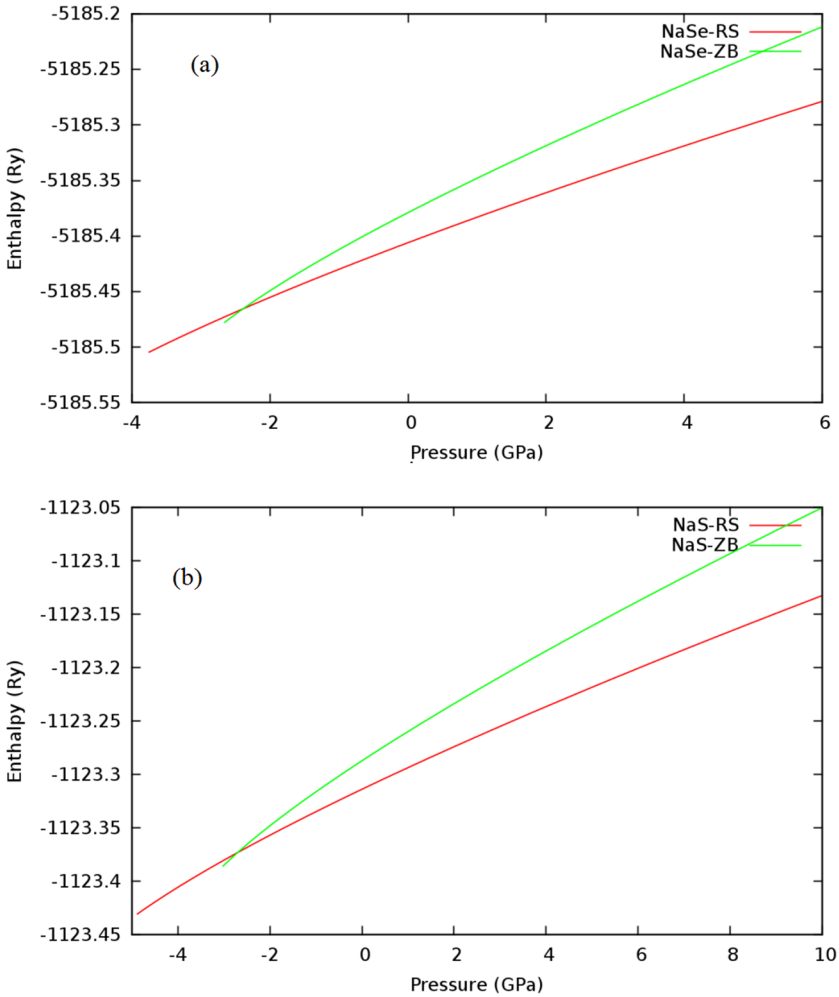

FIG. 2. Enthalpy as a function of pressure for (a) NaSe and (b) NaS compounds.

The rest of the paper is organized as follows: Sec. II presents the computational methodology, Sec. III presents the detailed results and discussions, and Sec. IV presents a summary of our findings and conclusions.

II. METHODOLOGY

Recently, calculations on the NaX (X = S and Se) compounds in the zincblende and rock salt crystal structures[19] were carried out by using the full-potential linearized augmented plane-wave

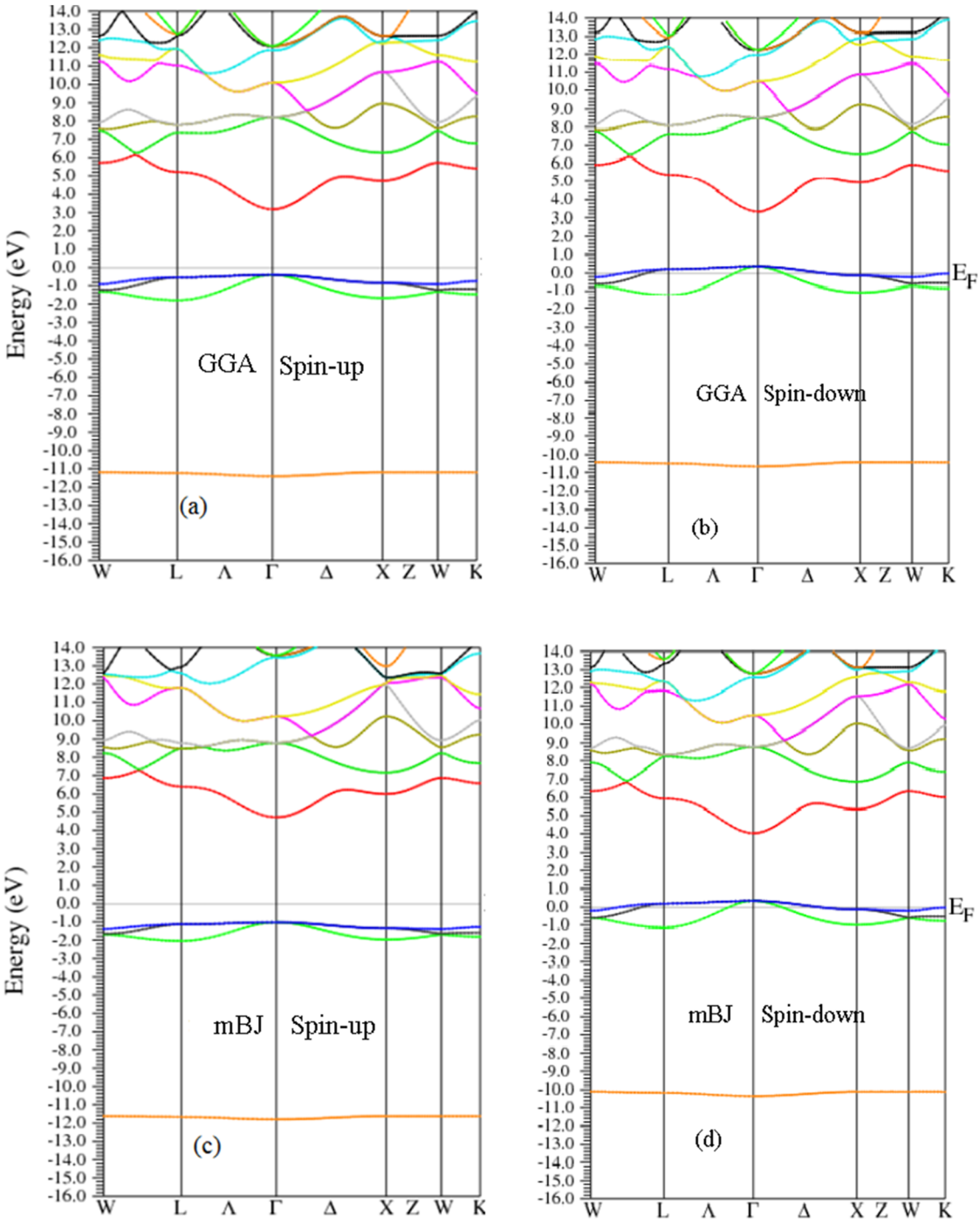

FIG. 3. Band structure of NaSe in the ZB structure (a) and (b) with PBE-GGA approximation and (c) and (d) with mBJ-GGA approximation.

(FP-LAPW) method.[20] FP-LAPW method is based on density-functional theory (DFT).[21] Generalized gradient approximation as parameterized in Perdew–Burke–Ernzerhof (PBE-GGA) scheme [22] has been carried out to predict and estimate the structural parameters, induced transition pressure, and magnetic properties. The modified Becke–Johnson (mBJ-GGA)[23,24] has been used to calculate the band structure for the NaX (X = S and Se) compounds. The products of the spherical-harmonic with both radial functions and radial functions' first derivative are used as the basis inside the muffin-tin (MT) spheres—an occupied space by spheres with radius R_{MT}; on the other hand, a plane-wave basis set is used in the interstitial region (remaining space outside the spheres). The total unit cell energy was

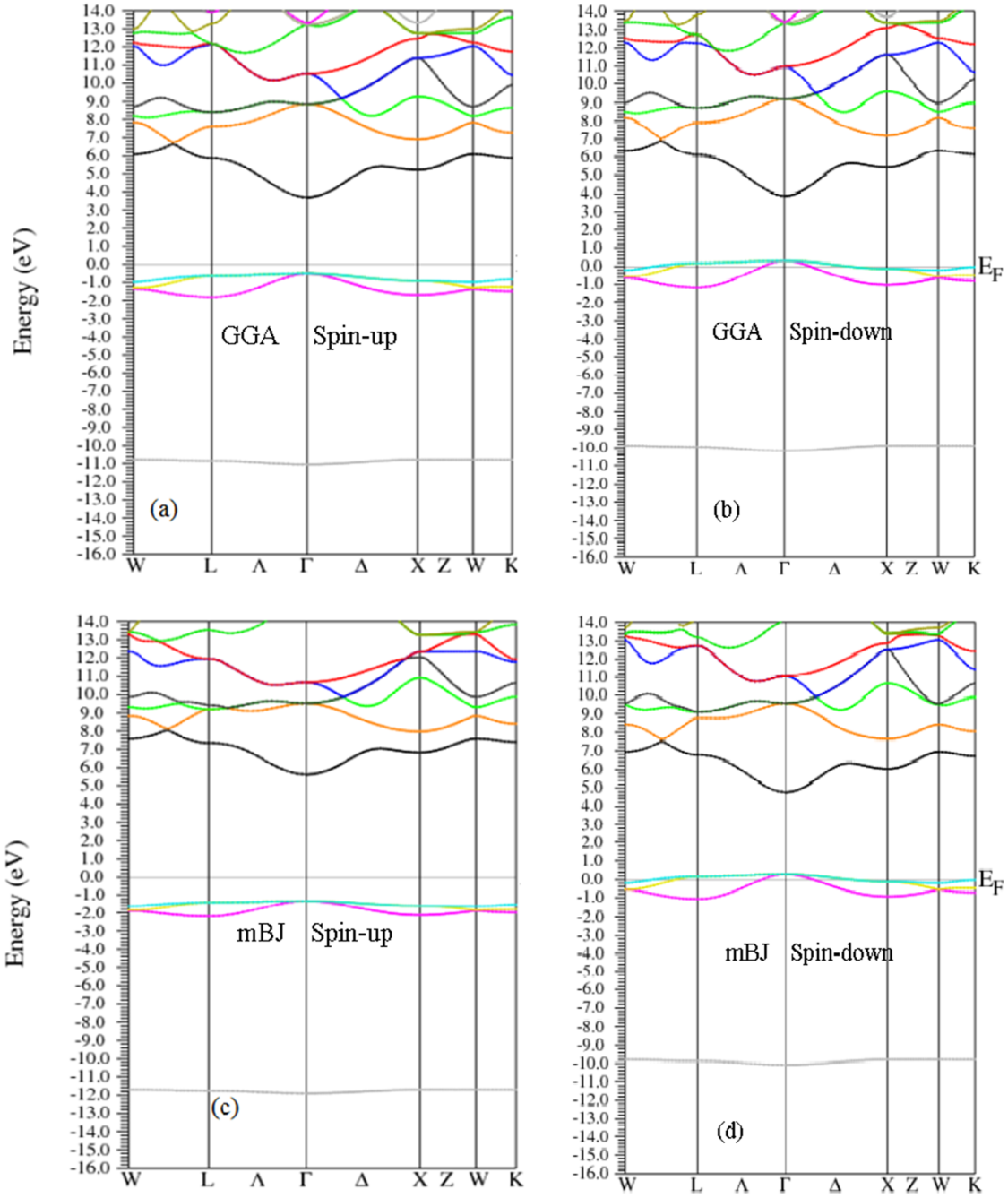

FIG. 4. Band structure of NaS in ZB structure (a) and (b) with PBE-GGA approximation and (c) and (d) with mBJ-GGA approximation.

minimized by using a grid size of 11 × 11 × 11 k-points, which is reduced to 56 k-points in the irreducible Brillouin zones (IBZ). The charge density was Fourier expanded up to G_{max} = 14, and the plane-wave cutoff was chosen such that $R_{MT} \times K_{max}$ = 8 with a cut-off l_{max} = 7. The iteration process was repeated until the calculated total energy per unit cell volume converged to less than 10^{-5} Ry/unit cell.

The valence electron configurations of studied atoms are Na ($3s^1$), S ($3s^2 3p^4$), and Se ($4s^2 3d^{10} 4p^4$).

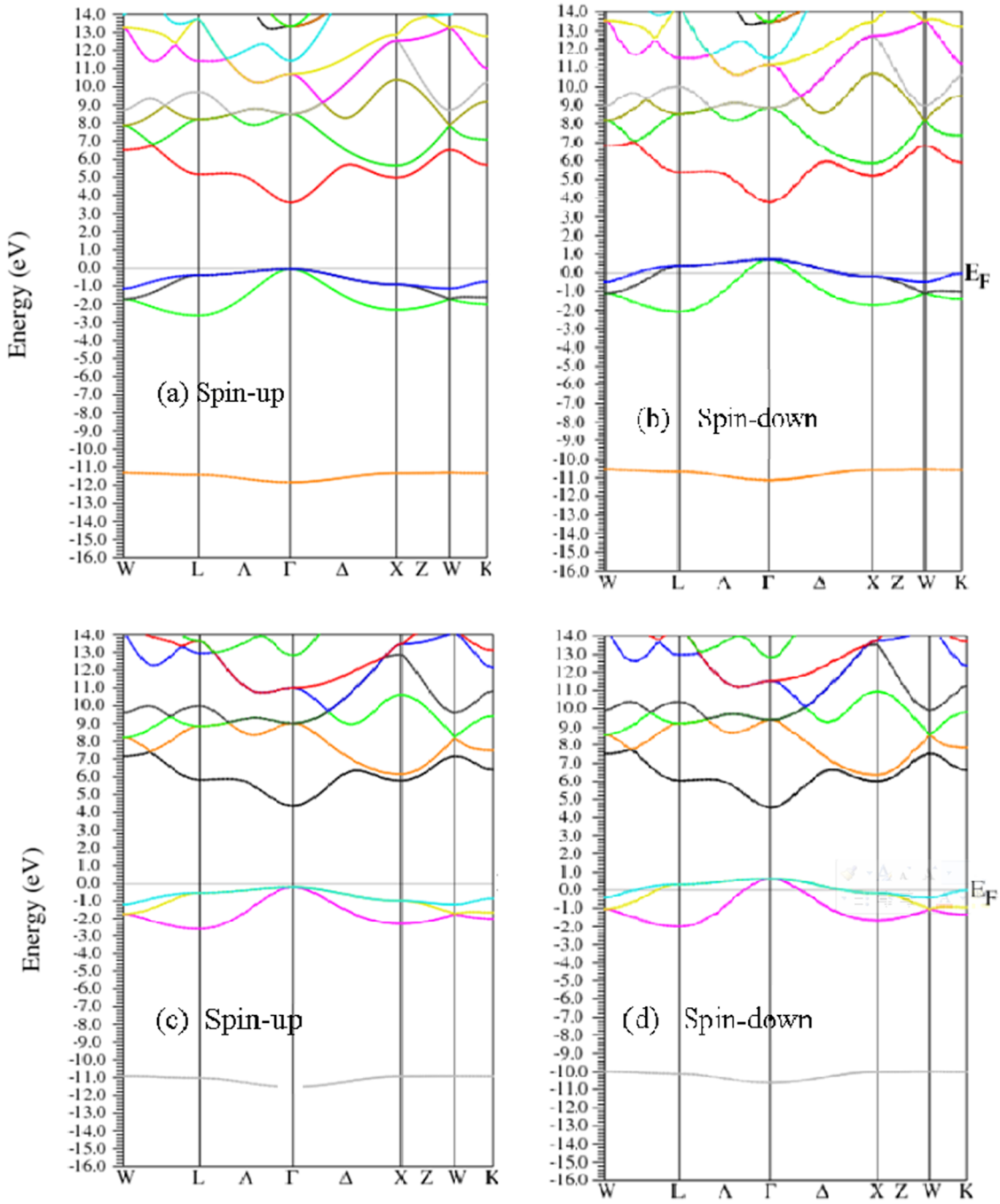

FIG. 5. Band structure of NaSe compound (a) spin-up and (b) spin-down configurations and NaS compound (c) spin-up and (d) spin-down configurations in the RS structure using the PBE-GGA method.

III. RESULT AND DISCUSSION

A. Structural properties

The ground state properties of the NaX (X = S and Sr) compounds in RS and ZB structures have been calculated by using the FP-LAPW method at the level of (PBE-GGA) scheme.[22] The total optimized energy at various unit cell volumes is computed and fitted to Murnaghan's equation of state (EOS),[25] as shown in Figs. 1(a) and 1(b) for both NaSe and NaS, respectively. It is clear from Fig. 1 that at ambient pressure, the RS structure has the lowest energy, i.e., the RS structure is the most stable under normal conditions.

Table I displays the calculated optimized lattice parameter (a_0), bulk modulus (B_0), and its first order pressure derivative (B'_0) for both chalcogenides, NaSe and NaS compounds, along with the available prior results.[17,19] The structural parameters a_0, B_0, and B'_0 are reasonably compatible with the prior results.[17,19] The lattice constants for NaX (X = S and Se) compounds within ZB and RS structures increase as the chalcogenide X radii increase. On the other hand, as the X radii increase, the B_0 decrease. ZB has the greatest lattice constant, while the RS has the greatest bulk modulus.

B. Phase transition

The calculated total energy as a function of unit cell volume for NaSe and NaS compounds is shown in Figs. 1(a) and 1(b), for both RS and ZB structures, respectively. It is clear from Fig. 1 that the RS structure, at ambient pressure, is the most stable ground state structure for both NaSe and NaS compounds. Under volume expansion, the calculations show that both NaSe and NaS compounds will experience a phase transition from RS to ZB structure. The pressure-induced structural phase transition can be estimated by analyzing the Gibbs free energy function (G) for each compound within the RS and ZB phases. Take $G = E_0 + PV + TS$. Since the theoretical calculations are done at $T = 0$ K, the last term in the Gibbs function (TS) has vanished and G resembles the enthalpy ($H = E_0 + PV$). The enthalpy vs pressure curves for NaSe and NaS compounds in the RS and ZB structures are displayed in Figs. 2(a) and 2(b). A phase transition occurs at the intersect point, where the enthalpies of the two phases have the same value and the pressure at this point is the induced transition pressure.

The bulk modulus (B_0) at equilibrium volume (V_0), its pressure derivative (B'_0), and equilibrium lattice constant (a_0) were

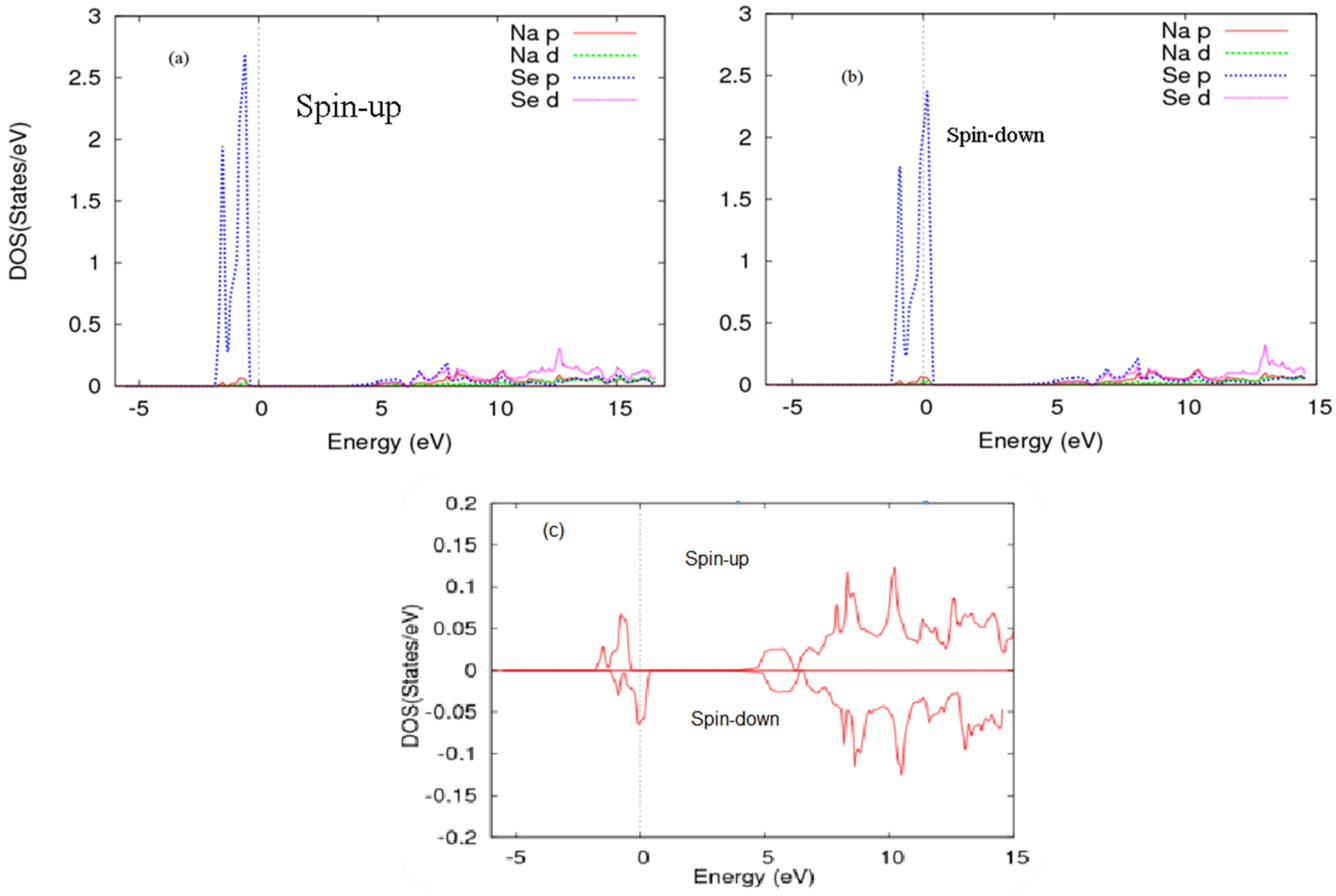

FIG. 6. Partial density of states within (a) spin-up, (b) spin-down, and (c) total density of states for NaSe compound in the ZB structure using the PBE-GGA approach.

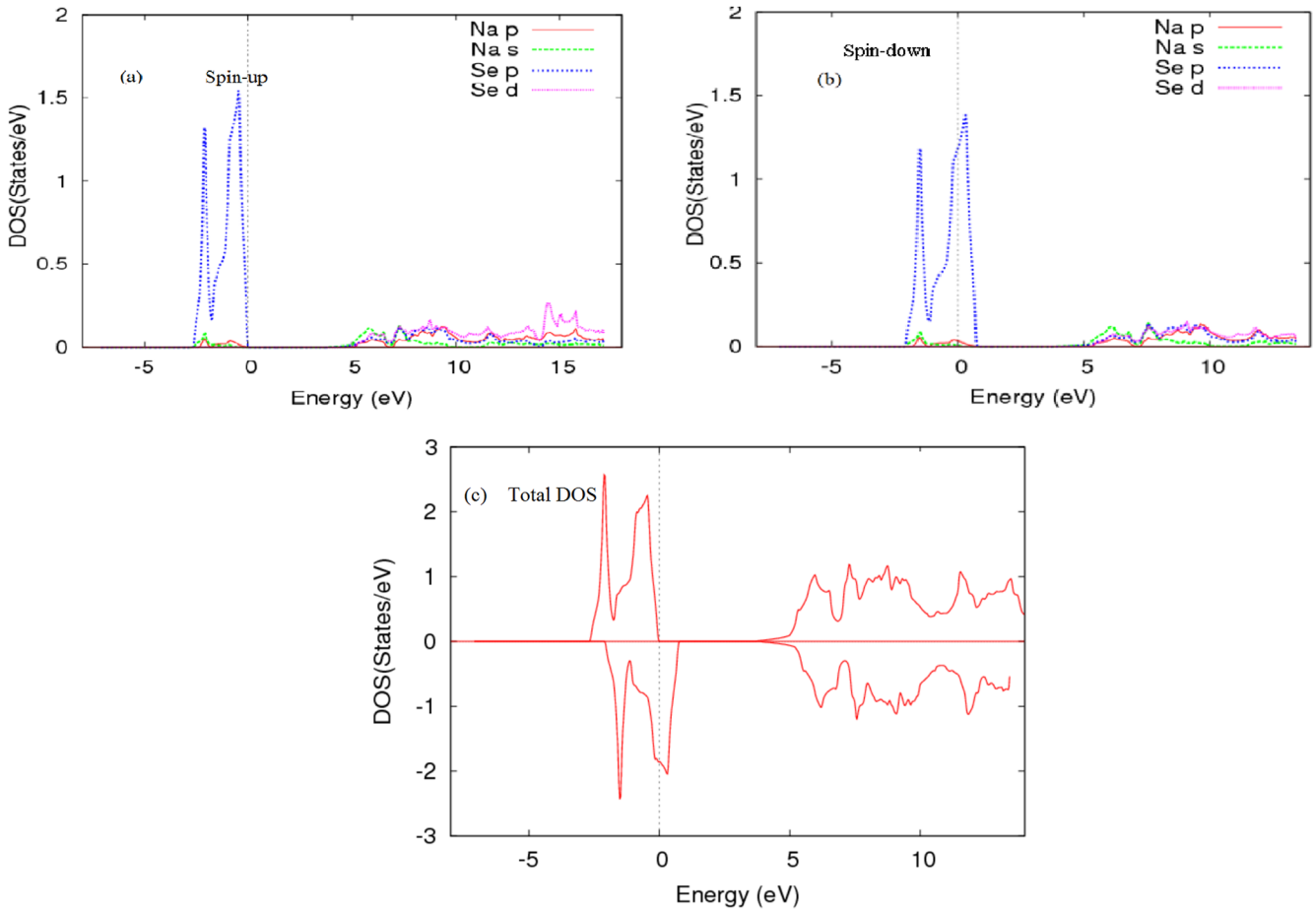

FIG. 7. Partial density of states within (a) spin-up, (b) spin-down, and (c) total density of states for NaSe compound in the RS structure using the PBE-GGA approach.

determined by fitting the total energy vs volume to Murnaghan's equation of states.[25] Murnaghan's equation of state is given by

$$E(v) = E_0 + \frac{B_0 V}{B_0'}\left[\frac{(\frac{V_o}{V})B_0'}{B_0' - 1} + 1\right] - \frac{B_0 V_0}{B_0' - 1}$$

where E_0 is the minimum energy.

The bulk modulus (B_0) and the pressure (P) are given by

$$B_0' = -\mathrm{V}\frac{dP}{dV} = \mathrm{V}\frac{d^2g}{dV^2}, \quad \mathrm{P} = -\frac{dE}{dV}.$$

The estimated transition pressures from RS to ZB structure for NaSe and NaS are about −2.40 and −2.77 GPa, respectively. This

TABLE II. Total and local magnetic moments of NaS and NaSe compounds in the ZB and RS structures.

Structure	Compound	M_{tot} (μ_B/unit cell)	M_{Na} (μ_B/unit cell)	M_X (μ_B/unit cell)	$M_{interstitial}$ (μ_B/unit cell)
ZB	NaS	0.999	0.001	0.735	0.254
	NaSe	1.0	0.014	0.683	0.303
RS	NaS	0.999	0.006	0.789	0.204
	NaSe	0.999	0.012	0.731	0.256

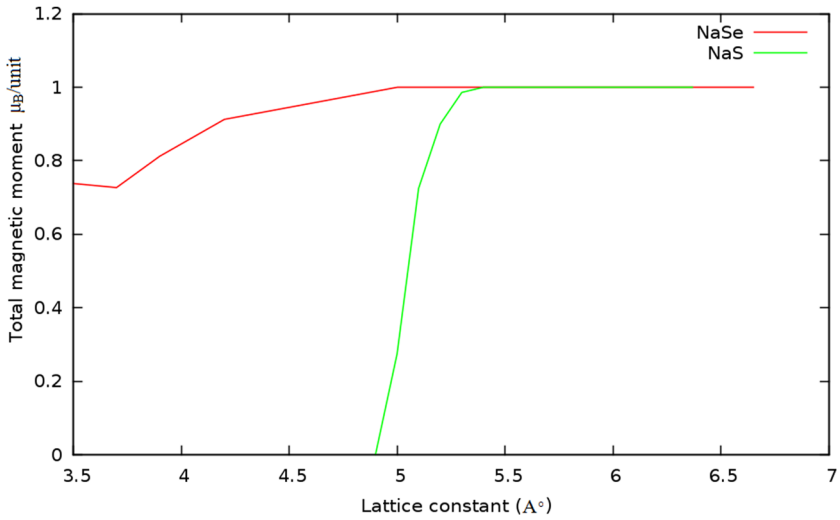

FIG. 8. Total magnetic moment vs lattice constant for NaS and NaSe compounds in the ZB structure.

means that the RS to ZB phase transition occurs for NaSe and NaS compounds under expansion.

The RS to ZB phase transition occurs when V/V_0 is greater than one, meaning that these two transitions require volume expansion. Negative pressure indicating an RS to ZB transition for both compounds means that we must expand the RS structure to get the ZB structure. In other meaning, we need larger pressure in the case of the expansion of RS into ZB. To the best of our knowledge, no theoretical or experimental values are available in the literature for the transition pressure from RS to ZB for both systems.

The negative of the slope of the common tangent line from RS to ZB is given by the transition pressure $P_t = -\frac{dE}{dV}$.

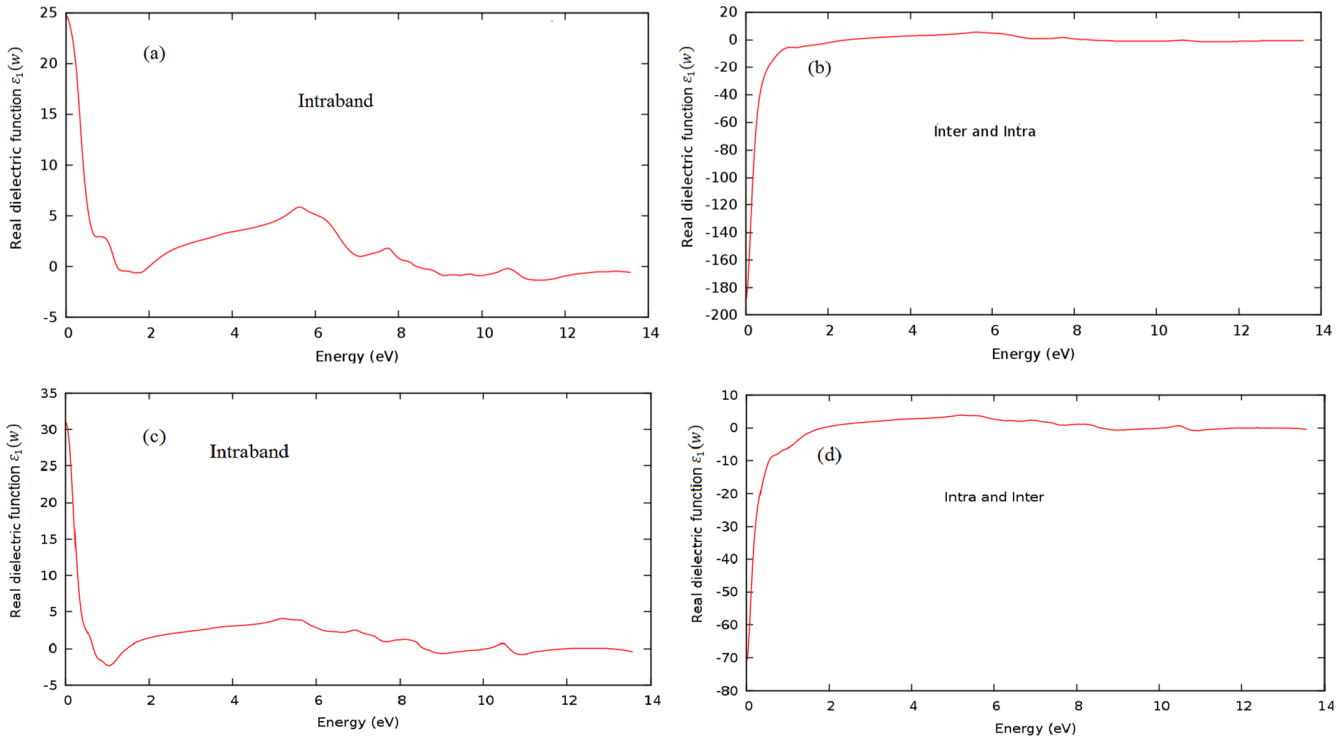

FIG. 9. Real part of the dielectric function $\varepsilon_1(w)$ of NaS compound (a) intraband transition and (b) inter- and intraband transition in the RS structure, and (c) intraband transition and (d) inter- and intraband transition in the ZB structure using the PBE-GGA approach.

C. Band structure and density of states

The electronic properties of NaX (X = S and Se) compounds in RS and ZB structures have been calculated by using the optimized lattice constant (a_0). The electronic properties have been employed to study their magnetic and optical characteristics. To understand the magnetic and optical properties of a material, it is necessary to know its electronic structure. The band structures of NaX (X = S and Se) compounds are calculated along the high symmetry lines in the irreducible Brillouin zone. Spin-polarized calculations are performed by using the concepts of spin-up/spin-down electrons.

Figures 3 and 4 illustrate the spin-polarized band structures of NaX compounds in the ZB structure for both spin-up (majority) and spin-down (minority) configurations. The majority spin shows a metallic behavior, and the bands are crossing the Fermi energy. On the other hand, the minority spin shows an insulating behavior, and the Fermi level is in between the valence and conduction bands, resulting in a direct bandgap (PBE-GGA: 3.51 eV; mBJ-GGA: 5.6 eV) and (PBE-GGA: 4.08 eV; mBJ-GGA: 7.0 eV) along the Γ high symmetry line for NaSe and NaS compounds, respectively. This implies that NaS and NaSe compounds in the ZB phase are half-metallic compounds and possess large HMF gaps. The mBJ-GGA approximation is used to treat exchange-correlation potential by implementing a nonlocal potential. The band structures of the NaS and NaSe compounds have a large bandgap in the minority channel coupled with the absence of an energy gap in the majority channel. The energy band gaps resulting from the mBJ approach are wider than GGA one, about 2.1 and 2.92 eV for NaSe and NaS compounds, respectively.

Figure 5 shows the band structures of NaX compounds in the RS structure for both spin-up and spin-down configurations by using the PBE-GGA method. The majority shows a metallic behavior, while the minority shows an insulating behavior, and the Fermi level is in between the valence and conduction bands, resulting in a direct bandgap of 3.6 and 4.24 eV along the Γ high symmetry line for NaSe and NaS compounds, respectively. This implies that NaS and NaSe compounds in the RS phase are half-metallic and possess large HMF gaps. As a result, the topologies of the energy band structure for NaS and NaSe compounds in the RS and ZB structures are quite similar. Furthermore, the topologies of the density of states (DOSs) for NaS and NaSe compounds are also quite similar. In this work, the DOS of the NaSe compound will only be displayed; DOSs of a system are used to describe the number of states/eV per each energy level that is possible to be occupied.

Figures 6 and 7 display the DOS of the NaSe compound in the ZB and RS structures, respectively. For further understanding of the nature of the band structures, the total and partial density of states (TDOS and PDOS) for NaSe compound in the ZB and RS structures have been calculated. The Fermi energy (F_E) indicated by a dotted horizontal line crosses the valence band for the spin-down configuration as seen in the band structure for the spin-down channel. For both spin-up and spin-down configurations, the valence energy bands arise mainly from the Se-p state, along with a very

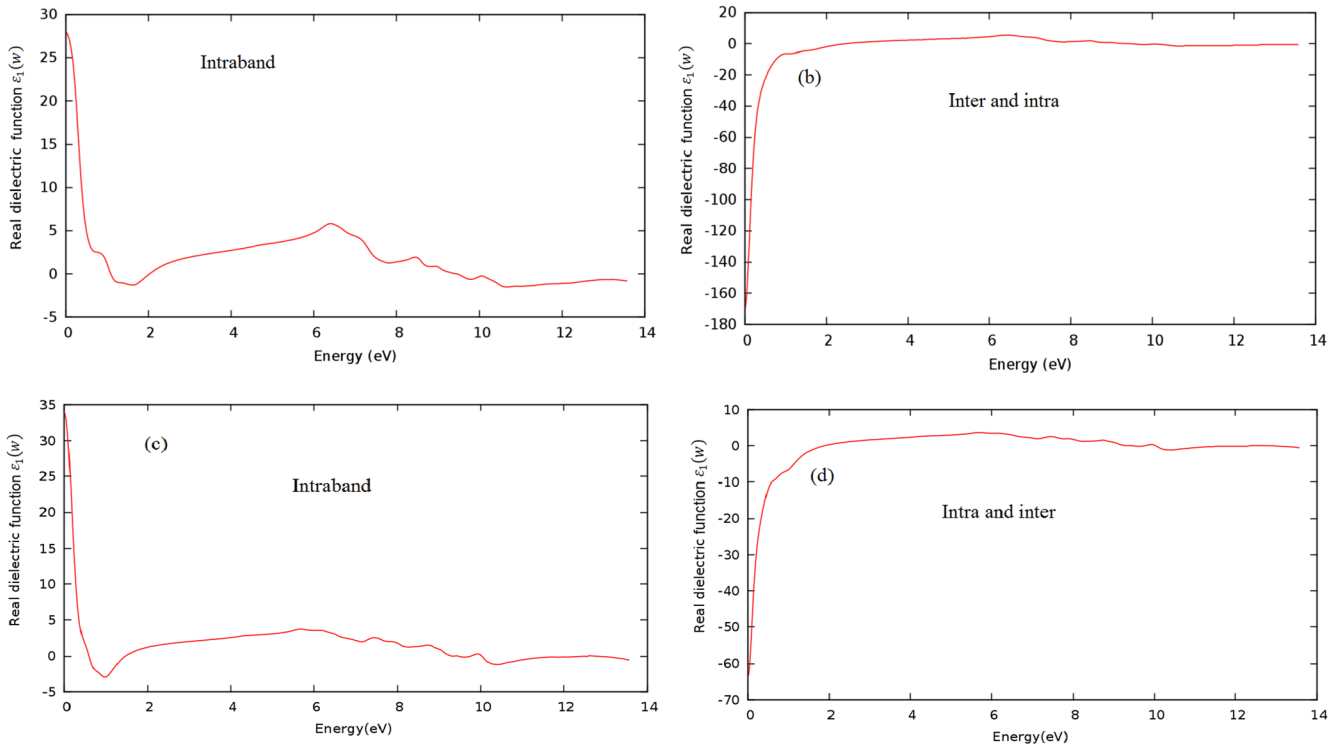

FIG. 10. Real part of the dielectric function $\varepsilon_1(w)$ of NaSe compound (a) intraband transition and (b) inter- and intraband transition in the RS structure, and (c) intraband transition (d) inter- and intraband transition in the ZB structure using the PBE-GGA approach.

small contribution from Na-p and Na-d states. Above the F_E, the conduction bands mainly originate from Se-d and Se-p states, with a small contribution from the Na-p and Na-d states.

D. Magnetic properties

The calculated total (M_{tot}) and local (M_X) magnetic moments for the NaSe and NaS compounds are presented in Table II. It shows that the calculated M_{tot} is ~1.0 μB/unit cell. The total and local magnetic moment is the same within mBJ and GGA methods, with an integer value for the total magnetic moment as expected for the HMF compounds according to Slater–Pauling curve. The M_{tot} for the two compounds is mainly referred to as the M_X of chalcogenides (S and Se) atoms. Our calculated magnetic moments agree well with previous calculations.[16,17,19]

In Fig. 8, we represent the variation in M_{tot} with the lattice constant in the ZB structure. The M_{tot} is invariant with the decrease in the lattice constant until a_0 = 5.35 and 4.5 Å for NaSe and NaS, respectively. Below these values, M_{tot} begins to decrease; M_{tot} for NaSe reaches zero at a_0 = 4.9 Å, while NaS stays to have a considerable value of M_{tot} even at a low lattice constant.

E. Optical properties

The FP-LAPW method is one of the best theoretical tools to calculate the optical properties of a compound. The optical properties are crucial to providing information about the internal structure of the NaX compounds. Moreover, the optical parameters are used to clarify the linear response of the electrons in the crystal to an external field. There are interactions between the electric field of the incident photon and the electrons in the crystal. These interactions cause optical transitions from occupied to unoccupied states. Since the investigated ZB and RS structures have a cubic symmetry, only one dielectric tensor component is needed to describe completely the linear optical response. The frequency dependent complex dielectric function $\varepsilon(\omega) = \varepsilon_1(\omega) + i\varepsilon_2(\omega)$ is known to describe the optical response of the medium at all phonon energies $E = \hbar W$, by using the formalism of Ehrenreich and Cohen.[26] $\varepsilon_1(\omega)$ and $\varepsilon_2(\omega)$ represent the real and the imaginary parts of the dielectric function, respectively. The imaginary part $\varepsilon_2(\omega)$ of the complex dielectric function in the long wavelength limit has been obtained by using the joint density of states (JDOS) and the transition matrix elements $M_{cv}(k)$,

$$\varepsilon_2(\omega) = \frac{e^2\hbar}{\pi m^2\omega^2}\sum_{v,c}\int_{BZ}|M_{cv}(k)|^2\delta[\omega_{cv}(k)-\omega]d^3k. \quad (1)$$

The integral here is only over the first Brillouin zone, and the matrix elements of dipole moments for direct transitions between conduction $[u_{ck}(r)]$ and valence $[u_{vk}(r)]$ bands are given by $M_{cv}(k) = \langle u_{ck}|e\cdot\nabla|u_{vk}\rangle$, where e represents the polarization of the electric

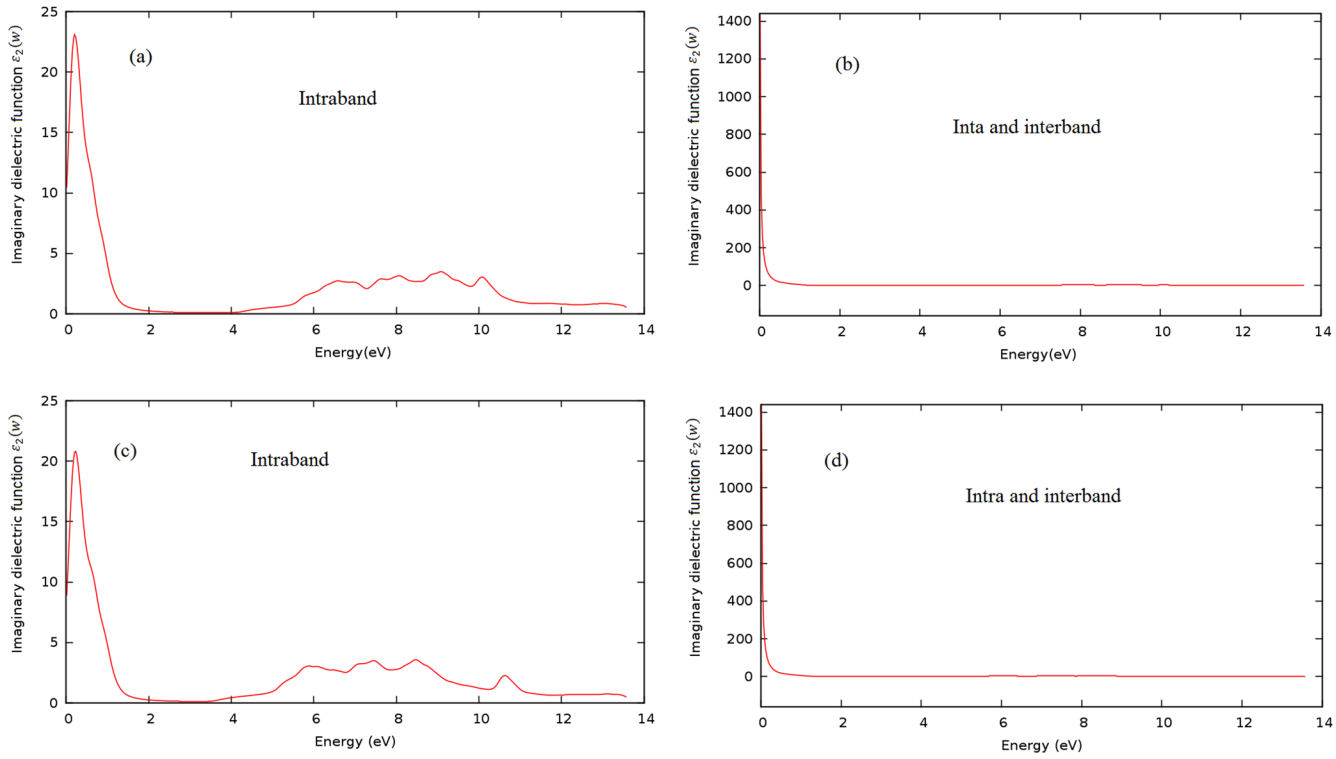

FIG. 11. Imaginary part of the dielectric function $\varepsilon_2(w)$ of NaS compound (a) intraband transition and (b) inter- and intraband transition, and for NaSe compound (c) intraband transition and (d) inter- and intraband transition in the ZB structure using the PBE-GGA approach.

field and is the excitation energy. The real part $\varepsilon_1(\omega)$ of the dielectric constant can be deduced from the $\varepsilon_2(\omega)$ by using the Kramers–Kronig transformation,

$$\varepsilon_1(\omega) = 1 + \frac{2}{\pi} P \int_0^{\infty} \frac{\omega' \varepsilon_2(\omega')}{\omega'^2 - \omega^2} d\omega', \tag{2}$$

where P denotes the Cauchy principal value of the integral. The knowledge of the complex dielectric function, real and imaginary parts, allows one to predict the crucial optical parameters such as the refractive index $n(\omega)$, the extinction coefficient $k(\omega)$, energy loss function $L(\omega)$, the reflectivity $R(\omega)$, and absorption coefficient $\alpha(\omega)$ by using the following expressions:[27–29]

$$k(\omega) = \left(\frac{1}{2} \left[\sqrt{\varepsilon_1^2(\omega) + \varepsilon_2^2(\omega)} - \varepsilon_1(\omega) \right] \right)^{1/2} \tag{3}$$

$$L(\omega) = \frac{\varepsilon_2(\omega)}{\varepsilon_1(\omega)^2 + \varepsilon_2(\omega)^2} \tag{4}$$

$$R(\omega) = \left| \frac{\sqrt{\varepsilon(\omega)} - 1}{\sqrt{\varepsilon(\omega)} + 1} \right|^2 = \left| \frac{\sqrt{\varepsilon_1 + i\varepsilon_2} - 1}{\sqrt{\varepsilon_1 + i\varepsilon_1} + 1} \right|^2 \tag{5}$$

$$n(\omega) = \left(\frac{1}{2} \left[\sqrt{\varepsilon_1^2(\omega) + \varepsilon_2^2(\omega)} + \varepsilon_1(\omega) \right] \right)^{1/2} \tag{6}$$

$$\alpha(\omega) = \frac{\sqrt{2}\omega}{c} \left(\sqrt{\varepsilon_1^2(\omega) + \varepsilon_2^2(\omega)} - \varepsilon_1(\omega) \right)^{1/2}. \tag{7}$$

It is known that the calculations of the optical properties of materials request a dense mesh of uniformly distributed k-points. Hence, the Brillouin zone integration for the optical properties was performed with 328 k-point. The broadening is taken to be 0.15 eV.

Real parts of the dielectric constants are depicted in Figs. 9 and 10 for NaSe and NaS compounds. It is seen that the $\varepsilon_1(\omega)$ curve goes through zero from below when inter- and intraband transition is considered, while it goes through zero from above at intraband transition. The static dielectric constant $\varepsilon_1(0)$ is given by the low energy limit of $\varepsilon_1(\omega)$ [$\varepsilon_1(0)$ = 34 and 28 for ZB and RS phases of NaSe compound, respectively, and $\varepsilon_1(0)$ = 30 and 25 for ZB and RS phases of NaS compound, respectively]. It is necessary to emphasize that we do not include phonon contributions to the dielectric screening, and $\varepsilon_1(0)$ corresponds to the static optical dielectric constant ε_∞. The static real part of the dielectric $\varepsilon_1(0)$ has positive values for both NaSe and NaS compounds within the intraband, which shows an insulating character, while within inter- and intraband transition, it has large negative values, indicating a metallic character. The real part of the dielectric constant and electronic properties agree that the spin-up (intraband transition) shows an insulating behavior, while the spin-down (inter- and intraband transition) shows a metallic behavior. As the photon's energy increases, the real dielectric

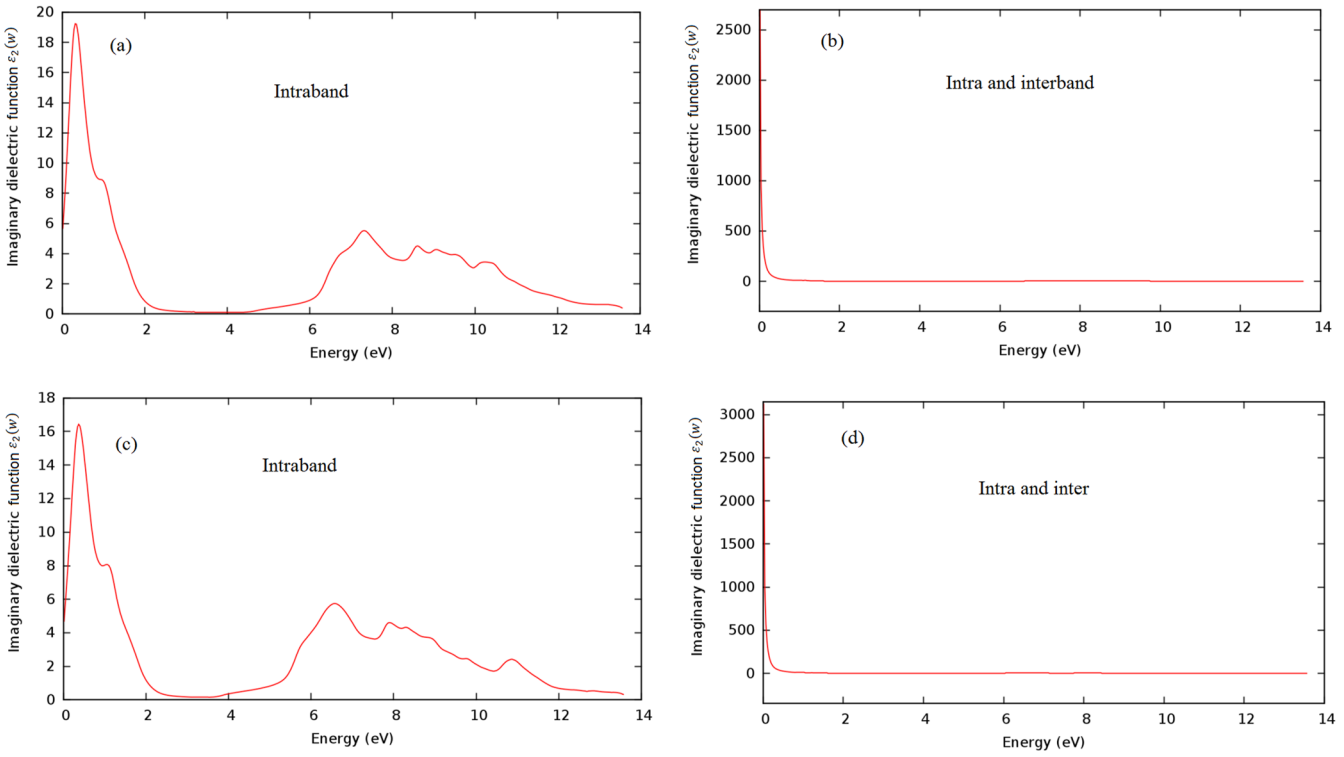

FIG. 12. Imaginary part of the dielectric function ε_2(w) of NaS compound (a) intraband transition and (b) inter- and intraband transition, and for NaSe compound (c) intraband transition and (d) inter- and intraband transition in the RS structure using the PBE-GGA approach.

functions within inter- and intraband transition have the same values within intraband transition. In high-frequency regions, the real dielectric functions within the two approaches become approximately equal to zero. The static dielectric constant $\varepsilon_1(0)$ for NaX compounds is negative within inter- and intraband transition. On the other hand, the static imaginary part of the dielectric constant $\varepsilon_2(0)$ for the two compounds, as shown in Figs. 11 and 12, has huge positive values within inter- and intraband transition in ZB and RS structures, respectively.

This suggests two remarkable facts: first, both NaSe and NaS compounds have a half-metallic characteristic, which agrees with the electronic structure calculations. Second, a negative value of $\varepsilon_1(\omega)$ at the energy less than 2 eV is pointing to the loss of light transit. The $\varepsilon_1(\omega)$ for both NaSe and NaS compounds has roots $(\varepsilon_1) = 0$, which occur at Plasmon oscillation. The compounds at these oscillations do not respond to the incident light. The sharp increase in $\varepsilon_1(\omega)$ with inter- and intraband transition at an energy range of 0–1.9 eV indicates a half-metallic behavior and this is related to the non-interaction between the incident photon and the compound at this energy range. When the photon energy is zero ($\omega = 0$), $\varepsilon_2(0)$ has a huge value with inter- and intraband transition, while it has a considerable value with the intraband transition. A sharp peak can be seen at the earlier beginning of the $\varepsilon_2(0)$ spectrum within the intraband transition, which is due to the transitions at the Γ-point symmetry. Sharp peaks followed by small peaks distributed along the $\varepsilon_2(0)$ spectrum are due to interband transitions. Since the intraband transition has an insulating behavior, these transitions are strongly related to the energy bandgap. The real and imaginary parts' behaviors are related to intraband contributions. In metal and half-metal (HM) systems, there are intraband contributions mainly from the conduction electrons; this contribution highly appears in the low-energy infrared part of the spectra. The calculated $\varepsilon_2(\omega)$ spectra show some peaks (threshold energy). These peaks in the imaginary part spectra are related to electron excitation. At these threshold energies, electron transitions from the occupied states in the valence band to the unoccupied states in the conduction band are observed. As shown in Figs. 11 and 12, a maximum transition from the valence band to the conduction band occurs at 0.30 and 0.2 eV for NaS and NaSe compounds, respectively. As can be seen, the $\varepsilon_2(\omega)$ spectrum does not vary greatly from NaSe and NaS compounds. This is attributed to the fact that the conduction bands' features and the symmetries of the wave functions, which dictate the selection rules and are fully reflected in the matrix moment elements, are somewhat similar. The refractive index $n(\omega)$ is an important physical

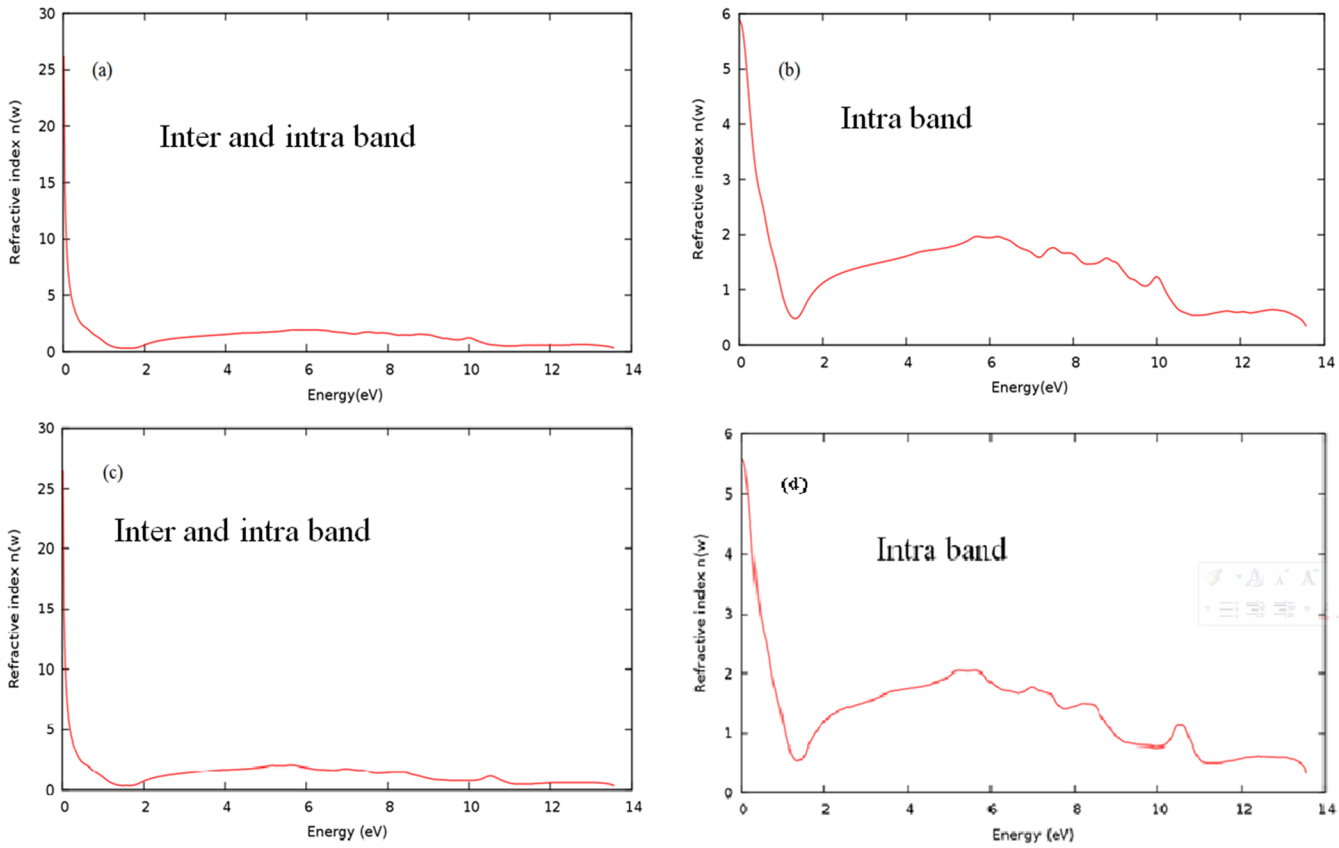

FIG. 13. Refractive index $n(w)$ of NaS with (a) inter- and intraband transition and (b) intraband transition, and that of NaSe compound with (c) inter- and intraband transition and (d) intraband transition in the ZB structure using the PBE-GGA approach.

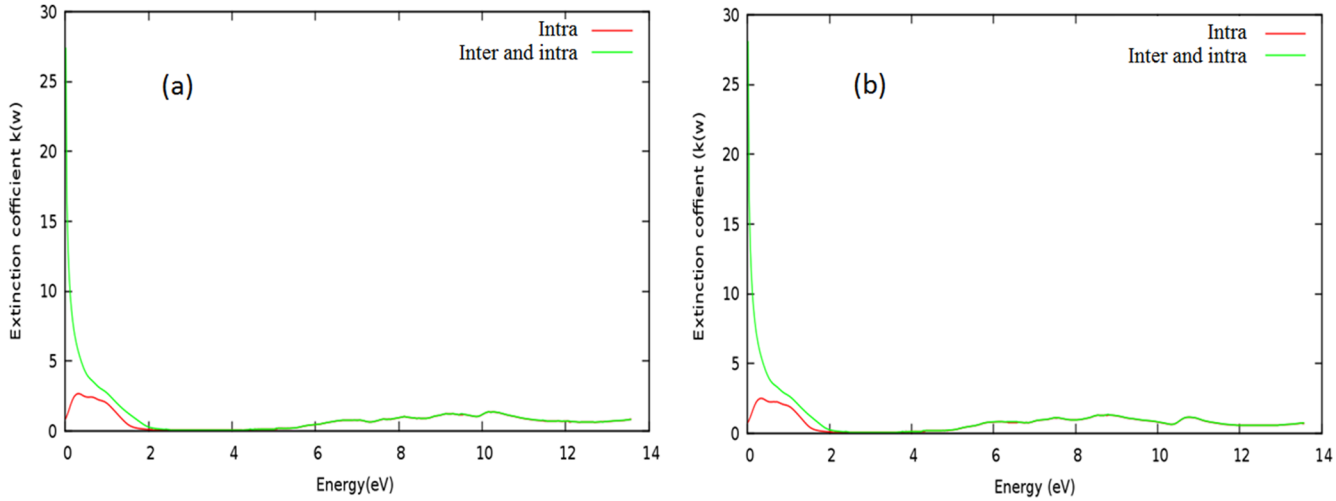

FIG. 14. Extinction coefficient k(w) for (a) NaS and (b) NaSe compounds in the RS structure using the PBE-GGA approach.

parameter. It is a frequency dependent function and closely related to the energy band structure. The refractive index $n(\omega)$ for NaS and NaSe compounds in the ZB structure are illustrated in Fig. 13.

The two compounds have the same behavior for inter- and intraband transition. Figures 13(a) and 13(c) show that $n(0)$ has a large value; $n(0) = 5.9$ and 6.0 for the interband transition of NaS and NaSe compounds, respectively, which indicate a metallic behavior as indicated by the real and imaginary parts of the dielectric constant. The trend is similar for the extinction coefficient $k(\omega)$ (see Fig. 14); $k(0)$ within inter- and intraband transition has a huge value compared with $k(0)$ within the intraband transition.

As the energy of incident photons increases, $n(\omega)$ and $k(\omega)$ drop to a lower value. Both $n(\omega)$ and $k(\omega)$ at high energy have the same values within the intraband transition and within inter- and intraband transition. The extinction coefficient $k(\omega)$ and the imaginary part of dielectric constant $\varepsilon_2(\omega)$ vary in the same way because $k(\omega)$ depends on the amount of absorption of photon when it propagates in the material. On the other hand, the refractive index $n(\omega)$ indicates the phase velocity of the electromagnetic wave.

Both $n(\omega)$ and $k(\omega)$ have small peaks along the spectrum. These peaks originate from electrons' transitions from the valence to conduction bands.

The reflectivity coefficient $R(\omega)$ spectra of NaS and NaSe compounds as a function of the frequency of photons in the RS structure are shown in Fig. 15. The reflectivity $R(\omega)$ is an important parameter since it displays the percent of reflected photons (energy) at the solid surface. The values of static reflectivity $R(0)$ of NaS and NaSe compounds within intraband transition are 51% and 50% (93% and 94% within inter- and intraband transition), respectively. A large static reflectivity indicates a metallic behavior; it implies that both NaS and NaSe compounds can be used as excellent coating materials in the infrared region. The reflectivity of the two compounds drops to zero

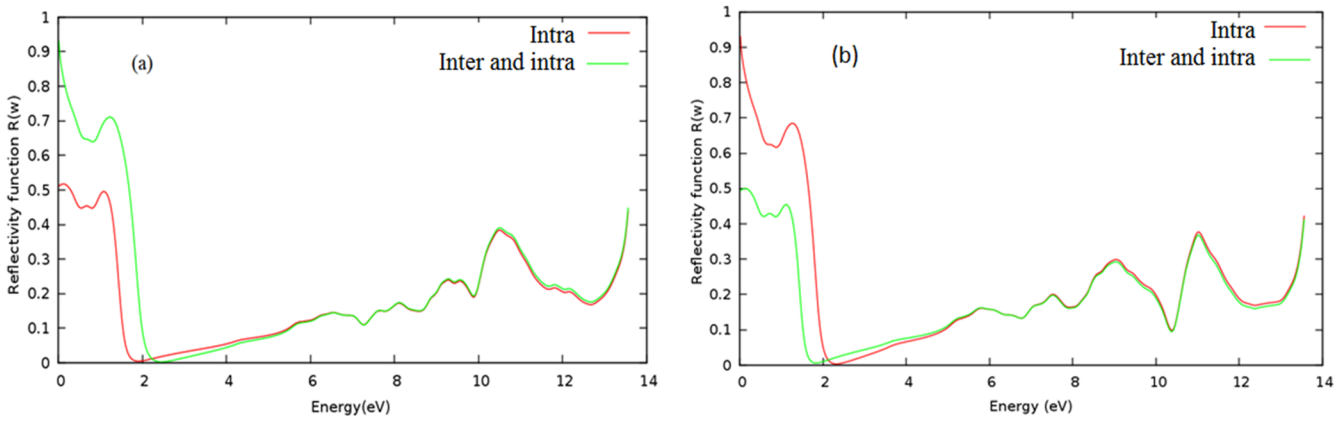

FIG. 15. Reflectivity function R(w) for (a) NaS and (b) NaSe compounds in the RS structure using the PBE-GGA approach.

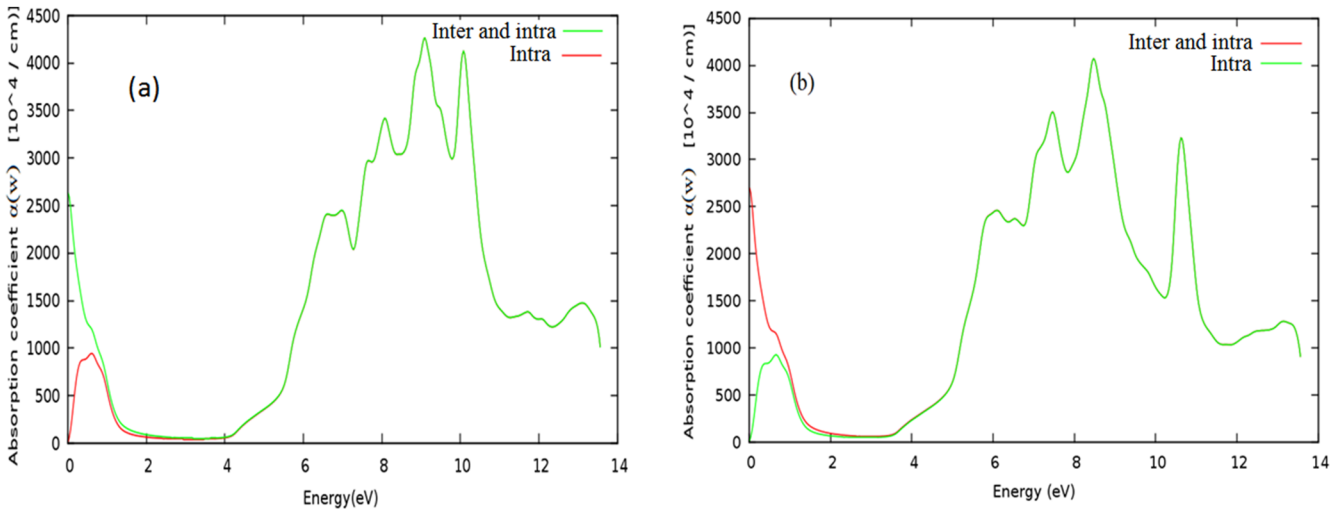

FIG. 16. Absorption coefficient $\alpha(w)$ (a) NaS and (b) NaSe compounds in the RS structure using the PBE-GGA approach.

value at photon energy of around 2 eV and then begins to increase again.

The absorption coefficient $\alpha(\omega)$ spectra of NaS and NaSe compounds are plotted in Figs. 16(a) and 16(b), respectively. NaS and NaSe compounds have a wide absorption region, are good absorbent materials, and their maximum absorption spectra are situated in the infrared and ultraviolet regions.$\alpha(0)$ is large, and as the photon energy increases, $\alpha(\omega)$ decreases and it reaches zero at around 2 eV. Above 4.0 eV, the absorption increases at certain peaks along the spectrum as the photon energy increases. The observed peaks in the absorption spectra are correlated with the peaks in the (ε_2) spectrum. As a result, they are connected to electron transitions from conduction to valence bands. Sharp peaks are seen in the spectrum at the valance and conduction bands, which can be very far from one another. These two compounds are bad absorbers in the visible region but good absorbent materials in the infrared (low energy) and ultraviolet (high energy) regions, which is due to their metallic nature. The energy loss spectrum $L(\omega)$ is used to describe the energy loss of fast electrons propagating in the material. The $L(\omega)$ of NaS and NaSe compounds is depicted in Figs. 17(a) and 17(b). The energy loss spectra for NaS and NaSe compounds are approximately zero at the early beginning of the spectrum, which is related to the high reflectivity.

As the reflectivity decreases and $\varepsilon_2(\omega)$ increases, the energy loss increases. We observe prominent peaks occurring at 1.51 and 1.48 eV within intraband transition (1.9 and 1.84 eV within inter- and intraband transition). These peaks define the screened plasma frequencyω_p[29] and correspond to the abrupt reduction of the reflectivity spectrum $R(\omega)$ and the zero crossing of $\varepsilon_1(\omega)$.

IV. CONCLUSION

We have investigated the structural, electronic, magnetic, and optical properties of the NaS and NaSe compounds by using

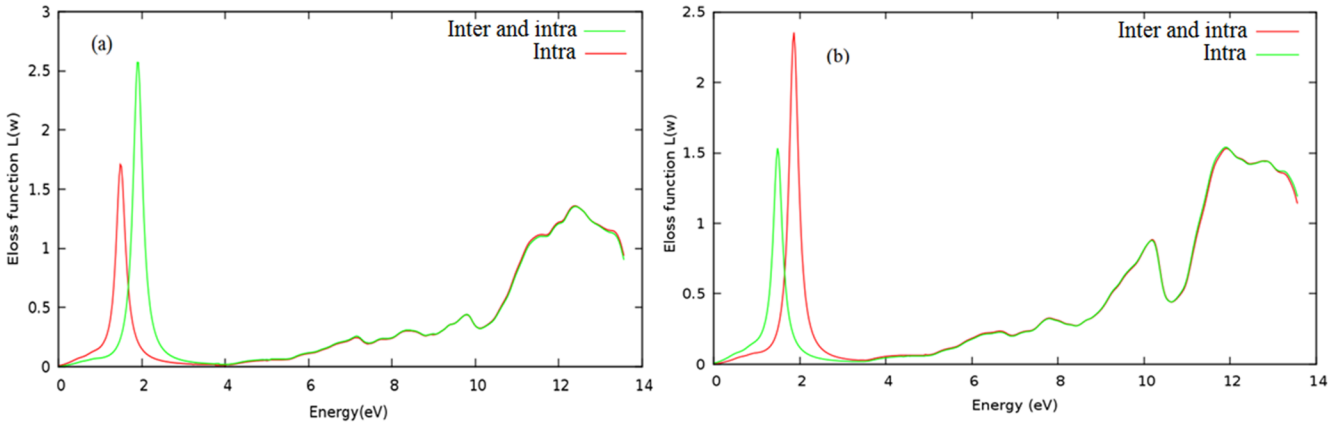

FIG. 17. Energy loss function L(w) for (a) NaS and (b) NaSe compounds in the RS structure using the PBE-GGA approach.

the PBE-GGA and mBJ-GGA approaches. It is found that these compounds are half-metallic ferromagnetic (HMF) compounds. The lattice constant increases as the chalcogenide atoms' (S and Se) radius increases, while the bulk modulus decreases. The band structures and the total density of states verify the half-metallic behavior of these compounds. The total magnetic moment M_{tot} per unit cell is equal to 1.0 μB. These compounds are half-metallic compounds since they have approximately an integer number of M_{tot}. The M_{tot} for NaS and NaSe is mainly attributed to the local magnetic moment of chalcogenide atoms (S and Se). It is invariant with decreasing the lattice constant until a_0 = 5.35 and 4.5 Å for NaSe and NaS, respectively. These two compounds show an insulating behavior with a spin-up configuration, while they show a metallic behavior with a spin-down configuration.

From optical calculations, we see that the $\varepsilon_1(0)$ value within the intraband transition is positive, which shows an insulating character, while within inter- and intraband transition, it has a large negative value, which shows a metallic character. The real part of the dielectric constant and the electronic properties agree that the spin-up is showing an insulating behavior, while the spin-down shows a metallic behavior. The imaginary part of the static dielectric function $\varepsilon_2(0)$ for the two compounds is a huge positive value within inter- and intraband transition. The sharp peak seen at the earlier beginning of $\varepsilon_2(0)$ spectrum within the intraband transition is caused by transitions at the Γ-point symmetry.

The $n(\omega)$ for both NaS and NaSe compounds indicates a metallic behavior as the $\varepsilon_1(\omega)$ and $\varepsilon_2(\omega)$ indicate. In the same view for the extinction coefficient $k(\omega)$, as the incident photons energy increases, the $n(\omega)$ and $k(\omega)$ values decrease, and both have the same values within intraband transition and within inter- and intraband transition. The extinction coefficient $k(\omega)$ and the imaginary part of dielectric constant $\varepsilon_2(\omega)$ vary in the same way because $k(\omega)$ depends on the amount of absorption of photon when propagates in the material. Both $n(\omega)$ and $k(\omega)$ have a small peak along the spectrum, which are originating from electrons' transitions from the valence to conduction bands. Both $k(\omega)$ and $\varepsilon_2(\omega)$ vary in the same way because $k(\omega)$ counts on the amount of absorption of photons when propagating in the medium. Furthermore, both $n(\omega)$ and $k(\omega)$ have small peaks along the spectrum, originating from the electrons' transitions between the valence and conduction bands.

The values of static reflectivity $R(0)$ of NaS and NaSe compounds within intraband transition are 51% and 50% (93% and 94% within inter- and intraband transition), respectively, which reflects a metallic behavior. It implies that both NaS and NaSe compounds can be employed as excellent coating materials in the infrared zone.

AUTHOR DECLARATIONS

Conflict of Interest

The authors have no conflicts to disclose.

Author Contributions

Raed T. Jaradat: Data curation (equal); Formal analysis (equal); Investigation (equal); Methodology (equal); Software (equal); Writing – original draft (equal). **Mohammed S. Abu-Jafar**: Conceptualization (equal); Investigation (equal); Methodology (equal); Project administration (equal); Supervision (equal); Visualization (equal); Writing – review & editing (equal). **Mahmoud Farout**: Data curation (equal); Formal analysis (equal); Methodology (equal); Software (equal); Writing – original draft (equal). **Said M. Azar**: Funding acquisition (equal); Methodology (equal); Software (equal); Writing – review & editing (equal). **Rabah Khenata**: Formal analysis (equal); Investigation (equal); Validation (equal); Visualization (equal); Writing – review & editing (equal). **Ahmad A. Mousa**: Data curation (equal); Formal analysis (equal); Investigation (equal); Methodology (equal); Software (equal); Validation (equal); Writing – review & editing (equal).

DATA AVAILABILITY

The data that support the findings of this study are available from the corresponding author upon reasonable request.

REFERENCES

[1] S. Wolf *et al.*, Science **294**, 1488 (2001); D. Awschalom and J. Kikkawa, Phys. Today **52**(6), 33 (1999).
[2] W. E. Pickett and J. S. Moodera, "Half metallic magnets," Phys. Today **54**(5), 39 (2001).
[3] Ph. Mavropoulos and I. Galanakis, "A review of the electronic and magnetic properties of tetrahedrally bonded half-metallic ferromagnets," J. Phys.: Condens. Matter **19**, 315221 (2007).
[4] R. A. de Groot *et al.*, "New class of materials: Half-metallic ferromagnets," Phys. Rev. Lett. **50**(25), 2024–2027 (1983).
[5] S. Ishida, T. Masaki, S. Fujii, and S. Asano, "Theoretical predicts of half-metallic compounds with the $C1_b$ structure," Physica B **239**, 163–166 (1997).
[6] R. Weht and W. E. Pickett, "Half-metallic ferrimagnetism in Mn_2VAl," Phys. Rev. B **60**, 13006 (1999).
[7] Y. Dedkov, U. Rudiger, and G. Guntherodt, "Evidence for the half-metallic ferromagnetic state of Fe_3O_4 by spin-resolved photoelectron spectroscopy," Phys. Rev. B **65**, 064417 (2002).
[8] S. P. Lewis, P. B. Allen, and T. Sasaki, "Band structure and transport properties of CrO_2," Phys. Rev. B **55**, 10253 (1997).
[9] L. Kronik, M. Jain, and J. Chelikowsky, "Electronic structure and spin polarization of $Mn_xGa_{1-x}N$," Phys. Rev. B **66**, 041203R (2002).
[10] J. Hong and R. Q. Wu, "Magnetic ordering and x-ray magnetic circular dichroism of Co doped ZnO," J. Appl. Phys. **97**, 063911 (2005).
[11] W.-H. Xie, Y.-Q. Xu, B.-G. Liu, and D. G. Pettifor, "Half-metallic ferromagnetism and structural stability of zincblende phases of the transition-metal chalcogenides," Phys. Rev. Lett. **91**, 037204 (2003).
[12] I. Galanakis and P. Mavropoulos, "Zinc-blende compounds of transition elements with N, P, As, Sb, S, Se, and Te as half-metallic systems," Phys. Rev. B **67**, 104417 (2003).
[13] D. Dahliah *et al.*, "Theoretical investigation of the structural stabilities, elastic properties and band structure characteristics of platinum carbide," Phase Transitions **91**(3), 271–283 (2018).
[14] M. Abu-Jafar *et al.*, "Structural, electronic, mechanical and elastic properties of Scandium Chalcogenides by first-principles calculations," Phase Transitions **93**(8), 773–783 (2020).
[15] R. Han *et al.*, "Possible ferromagnetism in Li, Na, and K-doped AlN: A first-principle study," J. Magn. Magn. Mater. **326**, 45–49 (2013).
[16] G. Y. Gao, K. L. Yao, M. H. Song, and Z. L. Liu, "Half-metallic ferromagnetism in rocksalt and zinc-blende MS (M = Li, Na, and K): A first-principles study," J. Magn. Magn. Mater. **323**(21), 2652–2657 (2011).
[17] F. Ahmadian, "Half-metallic ferromagnetism in the rocksalt and zincblende NaX (X = O, S, Se, Te, and Po)," J. Supercond. Novel Magn. **25**, 1589–1596 (2012).
[18] M. Moradi, M. Rostami, and M. Afshari, "Half-metallic ferromagnetism in wurtzite MS (M = Li, Na, and K)," Can. J. Phys. **90**(6), 531–536 (2012).

[19]H. Sadouki *et al.*, "Prediction of half-metallicity in the NaS, NaSe, and NaTe alkali-metal chalcogenides using first principles," Int. J. Comput. Mater. Sci. Eng. **7**(13), 1850015 (2018).
[20]P. Blaha, K. Schwarz, P. Sorantin, and S. B. Trickey, "Full-potential, linearized augmented plane wave programs for crystalline systems," Comput. Phys. Commun. **59**, 399–415 (1990).
[21]P. Hohenberg and W. Kohn, "Inhomogeneous electron gas," Phys. Rev. **136**, B864–B871 (1964).
[22]J. P. Perdew, K. Burke, and M. Ernzerhof, "Generalized gradient approximation made simple," Phys. Rev. Lett. **77**, 3865–3868 (1996).
[23]A. D. Becke and M. R. Roussel, "Exchange holes in inhomogeneous systems: A coordinate-space model," Phys. Rev. A **39**, 3761 (1989).
[24]F. Tran and P. Blaha, "Accurate band gaps of semiconductors and insulators with a semi local exchange-correlation potential," Phys. Rev. Lett. **102**, 226401 (2009).
[25]F. D. Murnaghan, "The compressibility of media under extreme pressures," Proc. Natl. Acad. Sci. U. S. A. **30**, 244 (1944).
[26]H. Ehrenreich and M. H. Cohen, "Self-consistent field approach to the many-electron problem," Phys. Rev. **115**, 786 (1959).
[27]M. Fox, *Optical Properties of Solids* (Oxford University Press, New York, 2001).
[28]F. Wooten, *Optical Properties of Solids* (Academic Press, New York, 1972).
[29]H. Wang *et al.*, "Simulation of electronic density of states and optical properties of PbB_4O_7 by first-principles DFT method," Phys. Status Solidi B **246**, 437 (2009).